



Article

Improved Wave Equation Analysis for Piles in Soil-Based Intermediate Geomaterials with LRFD Recommendations and Economic Impact Assessment

Harish K. Kalauni ¹, Nafis Bin Masud ¹, Kam Ng ^{1,*} and Shaun S. Wulff ²

¹ Department of Civil and Architectural Engineering and Construction Management, University of Wyoming, 1000 E. University Avenue, Department 3295, Laramie, WY 82071, USA; kalaunih@gmail.com (H.K.K.); nmasud@uwyo.edu (N.B.M.)

² Department of Mathematics and Statistics, University of Wyoming, 1000 E. University Avenue, Department 3295, Laramie, WY 82071, USA; wulff@uwyo.edu

* Correspondence: kng1@uwyo.edu

Abstract: The Wave Equation Analysis of Pile Driving (WEAP) has been widely used to determine drivability, predict static resistance, and assure the integrity of piles in soils. Assigning static and dynamic properties of Soil-based Intermediate Geomaterials (S-IGMs) remains a challenge in WEAP, partly attributed to IGMs that act as transition geomaterials between soil and hard rock. Furthermore, reliable static analysis methods for unit resistance predictions are rarely available for driven piles in S-IGMs in the default WEAP method. To alleviate these challenges, this study presents improved WEAP methods for steel piles driven in S-IGMs, including proposed damping parameters and Load and Resistance Factor Design (LRFD) recommendations based on newly developed static analysis methods and the classification of S-IGMs. A back calculation approach is used to generate the appropriate damping parameters for S-IGMs for three distinct subsurface conditions utilizing a database of 34 steel H- and pipe piles. Newly developed WEAP and LRFD procedures are also recommended. Additional independent 22 test pile data are used to compare and evaluate the accuracy and efficiency of the proposed WEAP methods with the default WEAP method. Compared with the default WEAP, bearing graph analysis results revealed that the selected proposed WEAP method, on average, reduces the underprediction of pile resistances by 6% and improves the reliability with a 43% reduction in the coefficient of variation (COV). Calibrated resistance factors for the proposed WEAP method increase to as high as 0.75 compared to the current AASHTO recommendation of 0.50. An economic impact assessment reveals that the proposed WEAP method is more efficient than the default WEAP method as the average difference in steel weight for 32 test piles is 0.06 kg/kN, almost close to zero, reducing the construction challenges in the current engineering practice.

Keywords: soil-based IGM; quake; damping; smith parameters



Citation: Kalauni, H.K.; Masud, N.B.; Ng, K.; Wulff, S.S. Improved Wave Equation Analysis for Piles in Soil-Based Intermediate Geomaterials with LRFD Recommendations and Economic Impact Assessment. *Geotechnics* **2024**, *4*, 362–381. <https://doi.org/10.3390/geotechnics4020020>

Academic Editor: Raffaele Di Laora

Received: 7 February 2024

Revised: 12 March 2024

Accepted: 28 March 2024

Published: 1 April 2024



Copyright: © 2024 by the authors. Licensee MDPI, Basel, Switzerland. This article is an open access article distributed under the terms and conditions of the Creative Commons Attribution (CC BY) license (<https://creativecommons.org/licenses/by/4.0/>).

1. Introduction

In rocky mountain areas, pile foundations are frequently driven in intermediate geomaterials (IGMs) to achieve higher resistances to meet the need for loads, satisfy the requirements of the Load and Resistance Factor Design (LRFD), increase design effectiveness, and reduce construction difficulties. Transitional geomaterials, known as IGMs, have a high level of natural variability. However, the definition of these geomaterials varies depending on the different applications [1]. According to Clarke and Smith [2], Marinou [3], De Freitas [4], and Martin and Stacey [5], most definitions are based on unconfined compressive strength. The design and construction of bridge foundations are difficult and challenging due to significant geological variability and a need for standardized definitions of IGM [6]. The lack of dependable design methodologies and measured IGM

characteristics hindered reliable prediction of geotechnical resistance of driven piles in IGMs [7–11].

During the construction stage, pile performance in IGM is frequently assessed utilizing dynamic testing, such as the Pile Driving Analyzer (PDA) with a subsequent signal-matching analysis using the Case Pile Wave Analysis Program (CAPWAP) [12,13]. However, once a test or production pile is equipped with PDA sensors and driven by a pile hammer during construction, the PDA-CAPWAP analysis can be carried out. Before construction, pile-driving analysis using the 1D Wave Equation Analysis Program (WEAP) was carried out to determine pile driving and acceptance criteria to identify the appropriate penetration depth that would accomplish the desired pile resistance using GRLWEAP14 software. Furthermore, WEAP has been frequently employed as an affordable construction approach due to the increased expense of a pile load test. WEAP is commonly used to assess pile drivability, predict static resistance, and ensure the integrity of piles in geomaterials. This program simulates pile penetration for each hammer strike. It estimates total pile resistance, compressive and tensile stresses in a pile, pile drivability, and pile integrity by modeling the driving system, pile, and geomaterials. One of WEAP's key outputs, the bearing graph, calculates the ultimate pile resistance as a function of blow count. The pile type, drive mechanism, percentage, and distribution of shaft resistance, and, most crucially, the dynamic soil factors, quake, and damping values all affect the bearing graph analysis. The proper selection of damping and quake values in the bearing graph analysis is crucial for the creation of pile driving criteria. Despite the quality of the modeling of the pile and drive systems, the damping and quake values are neither inherent geomaterial qualities nor quantifiable from laboratory measurements. The damping and quake values have been established from historical pile load test data for soils but not for the soil-based IGM (S-IGM). Previous studies examined pile drivability on soil to predict geotechnical resistances [14–17]. In those studies, the observed pile resistance from static load tests [18,19] or dynamic load tests [20–23] were matched with the ultimate pile resistance from WEAP using a back-analysis approach. Those approaches are only limited to driven piles in soil, not S-IGM, which is different from soils as the classification system has been created for distinguishing S-IGMs from soil to improve the prediction of pile resistances [7,24]. The study conducted by Masud et al. [7] shows that if the undrained shear strength (s_u) of any fine-grained geomaterials is equal to or greater than 129 kPa, then it would be classified as a fine-grained soil-based IGM (FG-IGM). Furthermore, when an SPT N-value is equal to or greater than 58 blows/0.3 m, coarse-grained soil-based IGM (CG-IGM) is classified for pile resistance predictions [24].

The current WEAP procedure possesses challenges with assigning the static unit resistances and dynamic parameters for S-IGMs. This challenge is particularly true for CG-IGMs that frequently have Standard Penetration Test (SPT) N-values higher than the WEAP maximum permissible 60 blows/0.3 m. Additionally, there are no reliable static analysis methods in default GRLWEAP14 software for estimating unit resistance for driven piles in S-IGMs, and the suggested Smith parameters were first created using pile load test data in soils. In this study, the newly developed static analysis methods for driven piles in S-IGMs are adopted from the study conducted by Masud et al. [7,24]. New static analysis methods for predicting unit shaft resistance (q_s) and unit end bearing (q_b) in S-IGM were developed for different subgroups of CG-IGM and FG-IGM to reduce the uncertainties associated with the prediction of pile resistances in S-IGMs [7,24]. For instance, CG-IGM is further differentiated based on pile types (steel H piles and steel pipe piles), and FG-IGM is further divided into clay-based IGM and silt-based IGM based on grain size. This paper presents a comprehensive wave equation analysis of piles driven in S-IGM using GRLWEAP14 software version 2010–2014 [25] by incorporating classification criteria and proposed static analysis methods for S-IGMs developed by Masud et al. [7,24].

The back-calculation of the dynamic parameters for the S-IGMs is conducted using 34 dynamic pile load test results in S-IGMs collected from four different states: Wyoming, Montana, Idaho, and North Dakota. This study introduces newly developed dynamic

parameters for the S-IGMs in the improved WEAP analysis to increase the reliability of pile resistance prediction based on the proposed classification and new static analysis methods. Four different WEAP methods, namely WEAP SAD (default WEAP method), WEAP UWD (newly developed static analysis methods are used as input parameters for S-IGMs), WEAP UWR (newly developed static analysis methods and damping parameters for S-IGMs are used), and WEAP SAR (default SA method but newly developed damping parameters are used), are proposed in this study to evaluate the pile resistance predictions in S-IGMs. An additional 22 test piles are collected from the literature as an independent dataset for validating the proposed WEAP methods. The calibrated LRFD resistance factors (ϕ) are recommended for the proposed WEAP methods using the three probability-based methods, Factor of Safety Method (FOSM), First Order Reliability Method (FORM), and Monte Carlo Simulation (MCS), to achieve target reliabilities.

An economic impact study was conducted to assess the pile performances in shale using the GRLWEAP14 software by Islam et al. [10]. However, similar studies have yet to be conducted to evaluate the economic impact analysis for driven piles in S-IGMs. This study evaluates the economic impact of WEAP SAD and WEAP UWR methods for driven piles in S-IGM to reduce construction challenges in future engineering practice.

2. Existing Studies on Wave Equation Analysis of Pile Driving

The numerical solution of the one-dimensional wave equation was presented by Smith [26,27] and subsequently used by Goble and Rausche [28] to develop the wave equation analysis of pile driving. They used a combination of lumped masses, springs, and dashpots to simulate the pile, hammer, driving system, and soil conditions. The Smith model is the most common soil model used in WEAP. This model accounts for the static and dynamic soil behaviors, and the total soil resistance during pile driving is the summation of static and dynamic resistances. Since its introduction, WEAP has been widely used to determine drivability, predict static and ultimate pile resistances, evaluate hammer performance, and assure the integrity of piles in soils. The compatibility of driving equipment with the pile and geomaterial conditions can be easily analyzed using WEAP [29]. WEAP has proven to be a reliable method for dynamic pile analysis and an economical construction control method.

The accuracy of pile resistance prediction determined from the wave equation analysis is highly dependent on the dynamic soil parameters: quake values (Q_s and Q_t) and damping factors (J_s and J_t). The quake and damping parameters can be predicted from the results of Static Load Tests (SLT) and dynamic load testing utilizing the PDA with a subsequent signal-matching analysis using the CAPWAP. Several combinations of quake and damping factors can be obtained to match results from load tests and WEAP [30]. Several past studies have been performed to determine the dynamic parameters summarized in Table 1. Liang and Sheng [31] provided theoretical expressions for predicting the dynamic parameters of soil in terms of pile penetration velocities, accelerations, pile sizes, and soil properties. McVay and Kuo [32] expressed the dynamic soil parameters regarding the SPT N-value and hammer energy (E_r). It should be noted that these recommended dynamic parameters were developed for piles driven in soils. However, the dynamic parameters for piles driven in S-IGMs have yet to be investigated.

Table 1. Summary of dynamic parameters for soils from previous studies.

References	Dynamic Parameter			
	Q_s	Q_t	J_s	J_t
Smith [27]	2.5 mm	2.5 mm	0.16 s/m	0.49 s/m
Coyle and Gibson [33]	NA	NA	NA	$\frac{1}{V^N} \left(\frac{P_d}{P_s} - 1 \right)$
Coyle et al. [18]	2.5 mm	2.5 mm	0.66 s/m (clay) 0.16 s/m (sand) 0.33 s/m (silt)	0.03 s/m (clay) 0.49 s/m (sand and silt)
Hannigan et.al. [34]	2.5 mm	D/120 (very dense and hard soil) D/60 (soft soils)	0.66 s/m (cohesive soil) 0.16 s/m (non-cohesive soil)	0.49 s/m for all soils
Liang and Sheng [31]	$\frac{f_s r_0}{G} \ln \left(\frac{r_m}{r_0} \right)$	$\frac{1+\nu}{2E} p_y \left(\frac{D}{2} \right)$	1/3 of toe damping	$\frac{\rho}{3f_t} \left(2r_0 \frac{\dot{v}_p}{v_p} + 3v_p \right)$
McVay and Kuo [32]	$e^{\left(\frac{B}{A \frac{E_r}{N_s} - 1} \right)}$	$e^{\left(\frac{B}{A \frac{E_r}{N_t} - 1} \right)}$	$e^{\left(\frac{B}{A \frac{E_r}{N_s} - 1} \right)}$	$e^{\left(\frac{B}{A \frac{E_r}{N_t} - 1} \right)}$

Q_s = Shaft quake; Q_t = Toe quake; J_s = Shaft damping; J_t = Toe damping; NA = Not Available; V = Velocity of soil deformation; P_d = Peak dynamic load; P_s = Peak static load; N = Exponential power modification (0.2 for sand and 0.18 for clay); f_s = Unit shaft resistance; r_0 = Radius of pile; r_m = Radius of influence zone; G = Average shear modulus in the influence zone; ν = Soil Poisson’s ratio; E = Elastic modulus of soil; p_y = Yielding stress on cavity; D = Pile diameter (mm); ρ = Soil density; f_t = Unit toe resistance; \dot{v}_p = Pile penetration acceleration; v_p = Pile penetration velocity; A, B = Regression constants [27]; N_s = Weighted average skin SPT N-value; N_t = Weighted average toe SPT N-value; and E_r = Rated energy of SPT hammer.

Using 24 steel H-piles in Wyoming, WEAP analysis was performed to predict pile resistances based on Q_t values of D/120 for S-IGMs [35]. Since J_s for IGMs were unavailable, the authors assumed J_s values of 0.16 s/m for non-cohesive geomaterials, 0.65 s/m for cohesive geomaterials, and 0.33 s/m for silt-like geomaterials. $Q_s = 2.5$ mm and $J_t = 0.5$ s/m were used independent of the geomaterial and pile types. The analysis yielded a mean resistance bias (ratio of CAPWAP measured pile resistance to the WEAP predicted pile resistance) of 1.0 but a relatively high Coefficient of Variation (COV) of resistance biases of 0.30. However, this study was limited to only one state and used no new static analysis methods. Similarly, Islam et al. [10] used 46 test pile data from Kansas, Montana, Iowa, and Wyoming to back-calculate the dynamic parameters for piles driven in shale. However, no similar studies have been conducted to develop a WEAP procedure for driven piles in S-IGMs.

The existing SPT N-value-based (SA) method is widely used as a geomaterial input method in WEAP. However, the SA method poses a challenge as there is no option for assigning S-IGM as a geomaterial. Although the “Other” option can be used, the program does not assign q_s or q_b to the S-IGMs. The q_s and q_b need to be manually input into WEAP; however, this creates another challenge as reliable static analysis methods for predicting these unit pile resistances in S-IGMs are unavailable in the default WEAP method. S-IGMs often exhibit SPT N-values greater than the maximum allowable input of 60 in the SA method. In those cases, other geomaterial properties, such as the friction angle (ϕ) or unconfined compressive strength (q_u), can be used to describe the geomaterial, but these properties are usually unavailable. In addition, WEAP limits the maximum q_s and q_b assigned by the SA method to the geomaterials (Table 2), and for a past study performed for the Wyoming Department of Transportation (WYDOT), the catalog of geomaterial properties and CAPWAP-measured resistances prepared by Adhikari [35] suggested that the CAPWAP-measured q_s and q_b of the cohesive soil-based IGMs ranged from 52 kPa to 172 kPa and 3687 kPa to 10,677 kPa, respectively. These average q_s and q_b were 78 kPa and 6608 kPa, respectively, which are higher than the maximum q_s and q_b recommended for clay limited by the SA method (Table 2). Applying maximum q_s and q_b values could lead to the underprediction of pile resistances by WEAP for piles driven in S-IGMs. Therefore, a user-defined input of the unit resistances for soil-based IGMs in WEAP is recommended.

Table 2. Maximum unit shaft resistance and unit end bearing used in the SA method [35].

Soil Type	Unit Shaft Resistance, q_s (kPa)	Unit End Bearing, q_b (kPa)
Sand and Gravel	250	12,000
Clay	75	3240
Silts	75 (non-cohesive); 250 (cohesive)	6000

Table 3 summarizes the WEAP-recommended dynamic parameters for soil and hard rocks [35]. These recommended dynamic parameters were initially developed based on pile load test data in soils [36]. However, recommendations have yet to be provided for determining the dynamic parameters and unit pile resistance for S-IGMs. Thus, improved WEAP analysis methods are proposed to incorporate unit pile resistances using new static analysis methods and back-calculated dynamic parameters to predict ultimate pile resistances in S-IGMs.

Table 3. WEAP recommended quake and damping values [35].

Dynamic Parameter	Geomaterial Type	Pile Type	WEAP Recommended Value
J_s	Non-cohesive Soils	All Pile Types	0.16 s/m
	Cohesive soils		0.66 s/m
J_t	All soil types		0.5 s/m
Q_s	All soil types	All Types	2.5 mm
Q_t	All soil types, soft rock	Non-Displacement piles	2.5 mm
	Very dense or hard soils	Displacement piles	$D/120$
	Soils that are not very dense or hard	Displacement piles	$D/60$
	Hard rock	All Types	1 mm

J_s = Shaft damping; J_t = Toe damping; Q_s = Shaft quake; Q_t = Toe quake; D = Pile diameter or width.

3. Pile Load Test Data

This study is conducted using 34 usable historical test pile data collected from Wyoming, Montana, Idaho, and North Dakota (Table 4). The test pile data are considered usable because they contain relevant subsurface information, PDA and CAPWAP results, and pile, hammer, and driving information. Table 4 summarizes the state, project, pile location, pile type, total pile penetration, stroke height, blow count, and hammer type of 34 test piles. The relevant geomaterial properties like SPT N-value, unit weight (γ), s_u , ϕ , and q_u are obtained from the respective boring logs and geotechnical reports. Among 34 test piles, 25 are steel H-piles and 9 are steel pipe piles. The total pile penetration ranges from 5.9 m to 41.6 m. The stroke height ranges from 1.68 to 3.05 m. These 34 test piles are used to conduct the bearing graph analyses, improve WEAP input methods based on the developed new static analysis methods for S-IGMs by Masud et al. [7,24], and recommend new damping parameters for both CG-IGM and FG-IGM for three different Subsurface conditions.

Table 4. Summary of historical test pile data and relevant End of Driving (EOD) information.

State	Project	Location	ID	Pile Type	L (m)	Bearing IGM Layer	EOD Information			
							S (m)	B	Q _m (kN)	Hammer Types
MT	M FK Po. CK	P-4 at B-1 *	1 *	OEP 406 mm	14.4	FG-IGM	2.44	23	1416	ICE I-30
	Cottonwood Cr	P-3 at B-1 *	2 *	OEP 508 mm	41.6	FG-IGM	2.90	313	2888	ICE I-36
		P-47 at B-4 #	3	CEP 406 mm	9.8	CG-IGM	2.68	37	2895	ICE I-36
	Capitol Interchange	P-8 at B-5 #	4	CEP 406 mm	14.8	CG-IGM	2.68	32	2253	ICE I-36
		P-8 at B-1 #	5	CEP 406 mm	8.8	CG-IGM	2.65	48	2148	ICE I-30
		P-2 at B-1 #	6	CEP 406 mm	8.5	CG-IGM	3.05	60	2973	ICE I-30
		P-11 at B-5 #	7	CEP 406 mm	14.7	CG-IGM	2.90	74	2442	ICE I-30
		P-1 at B-1 #	8	CEP 406 mm	9.0	CG-IGM	2.87	30	2323	ICE I-36
	P-38 at B-4 #	9	CEP 406 mm	8.4	CG-IGM	2.68	44	2538	ICE I-30	
ID	US-95 WR B	P-10 at Pi-1 *	10 *	HP 360×174	12.7	FG-IGM	2.87	590	4217	ICE I-30
	SH-55 SR Bridge	P-3 at Pi-1 *	11 *	HP 360×174	17.1	FG-IGM	2.50	1158	4168	Del D 36-32
		P-1 at Pi-4 *	12 *	HP 360×174	6.1	FG-IGM	2.44	333	4191	Del D 36-32
		P-1 at Pi-5 *	13 *	HP 360×174	10.4	FG-IGM	2.32	144	3522	Del D 36-32
		P-10 at A-2 *	14 *	HP 360×174	10.1	FG-IGM	2.35	105	4178	Del D 36-32
		P-4 at A-1 *	15	HP 360×174	17.2	FG-IGM	1.95	420	4455	Del D 36-32
		P-1 at Pi-2 ^	16	HP 360×174	14.6	FG-IGM	2.41	71	3403	Del D 36-32
		P-2 at Pi-3 ^	17	HP 360×174	10.7	CG-IGM	2.35	72	3190	Del D 36-32
	SH-51 SR Bridge	P-1 at A-1 ^	18	HP 360×174	21.0	FG-IGM	2.56	73	2825	ICE I-30 V2
		P at A-2 ^	19	HP 360×174	21.0	FG-IGM	2.74	52	2578	ICE I-30 V2
SH-28 LR B	P-2 at A-1 ^	20	HP 360×132	12.5	CG-IGM	2.29	16	1721	Pileco 30-32	
SH-52 UPRR B	P-4 at A-1 ^	21	HP 360×174	13.1	CG-IGM	2.59	31	2234	ICE I-30 V2	
ND	Memorial Bridge	P-1 at Pi-10(N) ^	22	HP 360×152	27.4	CG-IGM	2.59	40	3044	Del D-36
		P-1 at Pi-10(S) ^	23	HP 360×152	29.6	CG-IGM	2.59	49	3015	Del D-36
WY	PB-Muddy Creek	P-1 at A-2 *	24 *	HP 310×79	16.3	FG-IGM	2.26	109	1695	Del D16-32
		P-1 at B-2 *	25 *	HP 310×79	10.8	FG-IGM	2.41	108	2006	Del D16-32
	PB-Beech Street	P-1 at A-2 *	26 *	HP 310×79	13.6	FG-IGM	2.07	62	1272	Del D16-32
		P-3 at A-2 *	27 *	HP 310×79	14.1	FG-IGM	2.32	82	1357	Del D16-32
	PBME (BS)	BS P-2 at A-2 *	28 *	HP 310×79	12.5	FG-IGM	1.77	35	1477	APE D 30-32
	Hunter Creek	P-3 at A-1 #	29	HP 310×79	5.9	CG-IGM	1.68	850	1090	MKT DE 40
		P-2 at A-1 ^	30	HP 310×79	11.0	CG-IGM	1.92	63	1010	MKT DE 40
	Elk Fork Creek	P-5 at A-2 ^	31	HP 360×108	12.2	CG-IGM	2.50	49	1802	ICE 42S
Clark's Fork	P-1 at A-2 #	32	HP 360×108	13.7	CG-IGM	2.13	119	1957	Del. D 19-42	
PBME (Parson Street)	PS P-4 at A-1 *	33 *	HP 310×79	22.3	FG-IGM	1.92	32	1481	APE D 30-32	
	PS P-3 at A-2 *	34 *	HP 310×79	21.3	FG-IGM	2.04	35	1446	APE D 30-32	

B = Bridge; LR = Lemhi River; BS = Beech Street; Cr. = Creek; Po. = Porcupine; PBME = Pine Bluffs Marginal EBL; SR = Snake River; L = Penetration length; Del = Delmag; A = Abutment; B = Bent; Pi = Pier; P = Test pile; S = Stroke height; B = Blow count (b/0.3 m); EOD = End of Driving; Q_m = CAPWAP measured pile resistance at EOD; HP = H pile; CEP = Closed end pipe pile; OEP = Open ended pipe pile; * = Subsurface Condition I; # = Subsurface Condition II; ^ = Subsurface Condition III.

4. Four WEAP Procedures for Bearing Graph Analyses

Bearing graph analyses are performed on all useable test piles using the default WEAP SAD method and three proposed WEAP UWD, WEAP SAR, and WEAP UWR methods. The term “SA” refers to the default SPT N-value-based method, and “UW” refers to the new static analysis methods developed for the S-IGMs by Masud et al. [7,24]. The “D” refers to the GRLWEAP14 software recommended dynamic parameters, and the “R” refers to newly recommended dynamic parameters determined from the back-calculation procedure for S-IGMs. These four WEAP methods are explicitly described in the following subsections, and a summary of different WEAP methods is given in Table 5.

Table 5. Summary of WEAP methods.

Method	Geomaterial Input for q_s and q_b	Quake	Damping
WEAP-SAD (Default)	SPT N-based (SA) Procedure	$Q_s = 2.5 \text{ mm};$ $Q_t = D/60 \text{ or } D/120$	$J_s = 0.16 \text{ s/m (Coarse);}$ $J_s = 0.66 \text{ s/m (Fine);}$ $J_t = 0.50 \text{ s/m}$
WEAP-UWD	Proposed Static Analysis Methods	$Q_s = 2.5 \text{ mm};$ $Q_t = D/120$	$J_s = 0.16 \text{ s/m (Coarse);}$ $J_s = 0.66 \text{ s/m (Fine);}$ $J_t = 0.50 \text{ s/m}$
WEAP-UWR	Proposed Static Analysis Methods	$Q_s = 2.5 \text{ mm};$ $Q_t = D/120$	Recommended J_s & J_t from Back-calculation
WEAP-SAR	SPT N-based (SA) Procedure	$Q_s = 2.5 \text{ mm};$ $Q_t = D/120$	Recommended J_s & J_t from Back-calculation

Q_s = Shaft quake; Q_t = Toe quake; J_s = Shaft damping; J_t = Toe damping; D = Pile Diameter (mm).

4.1. WEAP SAD Method

The SA method is programmed in WEAP to define the geomaterial profile and geomaterial properties using the SPT N value (N), unit weight (γ), friction angle (ϕ), and unconfined compressive strength (q_u). Since the WEAP SA method only allows input of $N \leq 60$ blows/0.3 m, it is difficult to define the S-IGMs that generally have $N > 60$ blows/0.3 m. An alternative procedure is thus proposed to define the S-IGMs in the default SA method for WEAP analysis as follows:

- $N \leq 60$: N and γ are used to define the geomaterial.
- $N > 60$ for coarse-grained soil-based IGM (CG-IGM): ϕ and γ are used to define the geomaterial.
- $N > 60$ for fine-grained soil-based IGM (FG-IGM): q_u and γ are used to define the geomaterial.

WEAP assigns the default “D” dynamic parameters based on geomaterial and pile size (Table 3). The percentage shaft resistance obtained from the drivability analysis is used in the bearing graph analysis.

4.2. WEAP UWD Method

The default SA input procedure is used to input soil properties to predict the shaft resistance of overburdened soils along each test pile. For the S-IGMs, the unit resistances determined using the newly developed equations (Table 6) are manually input via the “SA input form” for individual layers. The WEAP-recommended dynamic parameters (Table 3) are assigned to the soil and S-IGMs based on the description of S-IGMs and pile type. The new percentage shaft resistance determined from a drivability analysis is used as an input in a bearing graph analysis.

Table 6. Proposed static analysis methods for predicting unit resistances for driven piles in S-IGMs [7,24].

New Prediction Equations for S-IGMs	
S-IGM	Unit Shaft Resistance
ML-IGM (H-pile & Pipe pile)	$\hat{q}_s = \left[\frac{1.80}{1+44e^{-0.89 \frac{s_u}{P_a}}} \right] P_a$
CL-IGM (H-pile & Pipe pile)	$\hat{q}_s = \left[\frac{1.58}{1+47.6e^{-1.34 \frac{s_u}{P_a}}} \right] P_a$
CH-IGM (H-pile & Pipe pile)	$\hat{q}_s = \left[\frac{2}{1+50.4e^{-1.4 \frac{s_u}{P_a}}} \right] P_a$
CG-IGM (H-Pile)	$\hat{q}_s = \left[\frac{1.21}{1+12.62e^{-4.06 \left(\frac{\sigma'_{v'}}{P_a} \frac{58}{(N_1)_{60}} \right)}} \right] P_a$
CG-IGM (Pipe-Pile)	$\hat{q}_s = \left[\frac{\frac{\sigma'_{v'}}{P_a} \frac{58}{(N_1)_{60}}}{0.105+0.52 \frac{\sigma'_{v'}}{P_a} \frac{58}{(N_1)_{60}}} \right] P_a$
S-IGM	Unit End Bearing
FG-IGM (H-pile & Pipe pile)	$\hat{q}_b = \left[\frac{\frac{s_u}{P_a} \times \frac{D}{D_B}}{0.001+0.0027 \frac{s_u}{P_a} \times \frac{D}{D_B}} \right] P_a$
CG-IGM (H-pile & Pipe pile)	$\hat{q}_b = 93.76 P_a \left[\frac{p_a}{\sigma'_{v'}} \frac{(N_1)_{60}}{58} \right]^{0.22}$

$(N_1)_{60}$ = corrected SPT N values; s_u = undrained shear strength; $\sigma'_{v'}$ = Vertical effective overburden stress; P_a = atmospheric pressure = 101.3 kPa; D = pile dimension or diameter; D_B = total pile penetration; \hat{q}_s = predicted unit shaft resistance; and \hat{q}_b = predicted unit end bearing.

4.3. WEAP SAR Method

The default SA input procedure is used to input soil properties to predict the shaft resistance of overburdened soils along each test pile. For the S-IGMs, the geomaterial input procedures explained in the WEAP SAD method are used. The significant difference between the WEAP SAR and WEAP SAD methods is that in the WEAP SAR method, newly recommended damping parameters are used, but in WEAP SAD, default WEAP damping parameters are used. The newly proposed damping parameters are manually input for each geomaterial layer using the “pile segment” and “soil segment damping/quake” options in the WEAP.

4.4. WEAP UWR Method

Since the dynamic parameters and static resistance equations used by WEAP were initially developed for soils, the existing static analysis methods might not accurately determine the q_s and q_b for S-IGMs. Hence, the new static analysis methods (Table 6) developed by Masud et al. [7,24], authors from the University of Wyoming “UW”, are adopted to predict the q_s and q_b for the S-IGMs that are manually input into WEAP. The new percentage shaft resistance obtained from the drivability analysis is used in the bearing graph analysis. The recommended “R” dynamic parameters determined from the back-calculation procedure discussed in the next section are manually input into the bearing graph analysis through the “pile segment” and “soil segment damping/quake” options. For all WEAP methods, bearing graph analysis is conducted to predict the ultimate pile resistance using the field-reported hammer blow count and stoke height for each test pile shown in Table 5.

5. Back-Calculation Procedure for Dynamic Parameters

Pile resistance prediction from WEAP depends on selecting the quake values and damping factors. However, matching the pile resistance from CAPWAP with the predicted ultimate resistance from WEAP’s bearing graph analysis can yield a combination of quake

and damping parameters. Thus, back-calculation becomes an indeterminate problem that requires a reduction in unknown quake and damping parameters. A parametric study has been performed to determine the effect of the quake and damping parameters on the bearing graph [10]. The study found that the J_s have the most effect on the bearing graph.

On the other hand, the Q_s value has little effect on the bearing graph, and thus, the default Q_s value of 2.5 mm recommended in WEAP is adopted in this study for S-IGMs. Since S-IGMs are more rigid and stiffer than soil, it is reasonable to assume the WEAP-recommended Q_t value of $D/120$ (hard and stiff soils) for the S-IGMs. For the damping factors, a J_s -to- J_t ratio of one is assumed to create a determinate problem as pile resistance from WEAP depends on the relative effect of both damping factors. The bearing graph is generated by changing J_s and J_t for the S-IGM layers while considering the WEAP-recommended values for the overburdened soil layers. The predicted resistance from WEAP is determined using the stoke height and blow count at the End of Driving (EOD) given in pile driving reports. The best back-calculated damping factors are determined by matching the predicted ultimate resistance from WEAP with the resistance determined from CAPWAP at EOD until the difference is less than 0.1%. A sample calculation is illustrated using the HP 310×79 test pile (pile ID-26 from Table 4) at the Abutment 1 location of the Pine Bluff-Beech Street bridge project in Wyoming. The CAPWAP resistance of the test pile at EOD is 1272 kN at this particular location. The pile length, penetration, hammer, stroke height, and blow counts at the EOD are 15.3 m, 13.6 m, Delmeg D 16–32, 2.07 m, and 62 b/0.3 m, respectively. Pile resistance from WEAP methods depends on quake and damping values, creating an indeterminate problem. To eliminate this indeterminacy, the shaft quake Q_s value of 2.5 mm, toe quake Q_t value of 2.58 mm, and J_s -to- J_t ratio of 1 are chosen for the bearing graph analysis. After several trials and errors, the damping factor $J_s = J_t = 0.5$ s/m was finally selected for the bearing graph analysis, and the WEAP predicted a resistance of 1270.9 kips. The resistance difference between WEAP and CAPWAP at EOD is 0.09% in this test pile. Based on this methodology, all the back-calculated damping parameters for 34 test piles are determined.

5.1. Back-Calculation Results

The back-calculations show that the back-calculated damping parameters depend upon the bearing geomaterial and the overburden subsurface condition. Three subsurface conditions, I, II, and III, are proposed, along with the recommended damping factors for driven piles in S-IGMs. A flowchart to determine the different subsurface conditions based on geotechnical and boring log information is provided in Figure 1.

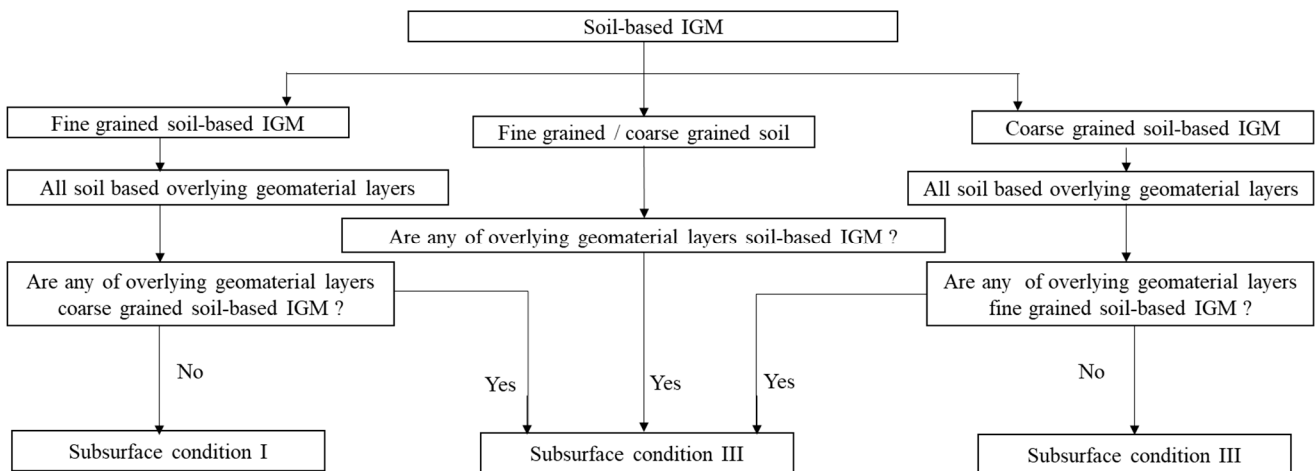


Figure 1. Flowchart to classify the subsurface conditions I, II, and III.

5.2. Subsurface Condition I (Fine-Grained Soil-Based IGM as Bearing Layer)

Out of the 34 test piles, 15 test piles are driven onto fine-grained soil-based IGMs (FG-IGMs) as the bearing layer. Subsurface condition I can be identified as having FG-IGM as the bearing IGM layer and overlying with one or more of either soil layers or FG-IGMs. No coarse-grained soil-based IGM (CG-IGM) is encountered in subsurface condition I. The back-calculated damping factors varied from 0.10 s/m to 1.23 s/m. The average back-calculated damping factor of 0.59 s/m for the FG-IGM is higher than the J_t of 0.50 s/m for cohesive soils, but lower than the J_s of 0.65 s/m for cohesive soils. The higher average back-calculated J_t and lower average back-calculated J_s indicate that the current WEAP-recommended J_t and J_s for cohesive soils will underpredict the shaft resistance and overpredict the end bearing of FG-IGMs. A relationship shown in Figure 2a is developed for the back-calculated damping factor based on the s_u (kPa) of FG-IGM at the pile tip and slenderness ratio (i.e., the ratio of pile penetration L (m) to pile dimension D_p (mm)). The fitted linear regression function for predicting \hat{J}_t (s/m) and \hat{J}_s (s/m) is given by Equation (1) with a relatively high coefficient of determination (R^2) of 0.74. Equation (1) infers that those piles with a deeper bearing FG-IGM layer will demand higher damping factors, but the damping factors will decrease with increasing pile size. Equation (1) covers $6.1 \text{ m} \geq L \geq 41.61 \text{ m}$, $129 \text{ kPa} \geq s_u \geq 672 \text{ kPa}$, and a wide range of pile sizes of HP 310 mm to 360 mm and 406 mm to 510 mm of open-ended pipe piles (OEP). Equation (1) is applicable for damping factor ranges from 0.1 s/m to 1.23 s/m.

$$\hat{J}_t = \hat{J}_s = 0.05 \frac{s_u \times L}{D_p} - 0.025 \tag{1}$$

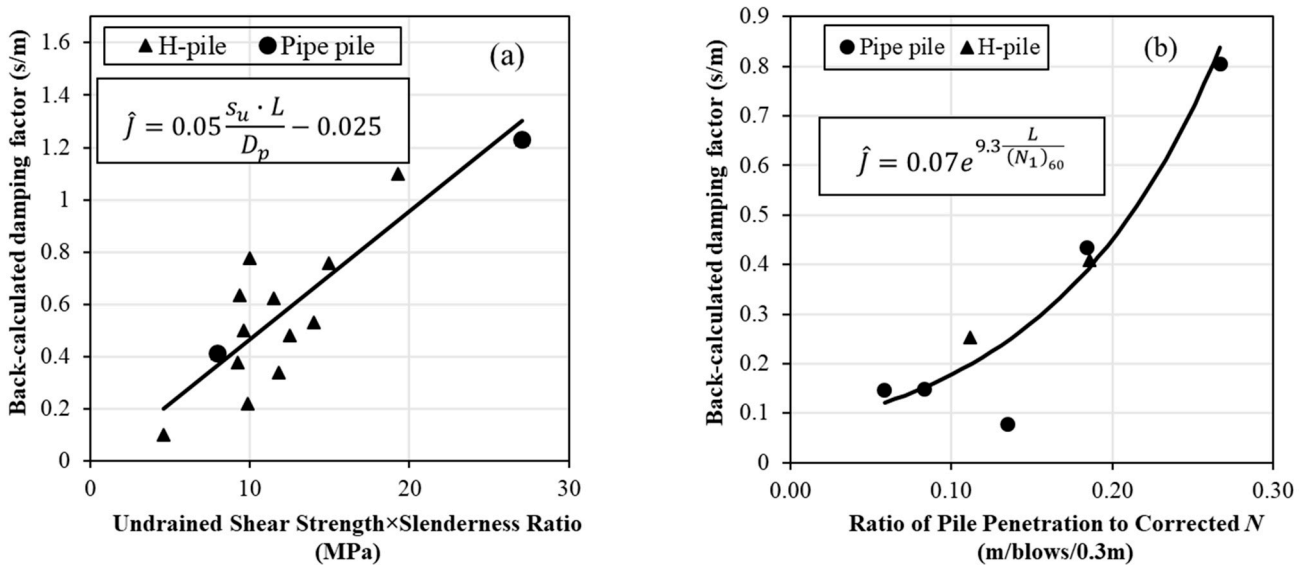


Figure 2. (a) Relationship between back-calculated damping factor and the product of undrained shear strength and slenderness ratio for FG-IGMs and (b) relationship between damping factor and the ratio of pile penetration to corrected SPT N-value for CG-IGMs.

5.3. Subsurface Condition II (Coarse-Grained Soil-Based IGM as Bearing Layer)

Nine test piles are driven onto coarse-grained soil-based IGMs (CG-IGM) as the bearing layer. Subsurface condition II can be identified as having CG-IGM as the bearing IGM layer and overlying with one or more of either soil layers or CG-IGMs. No FG-IGM is encountered in this subsurface condition II. The back-calculated damping factors ranged from 0.075 s/m to 0.82 s/m with the average back-calculated damping factor of 0.33 s/m. The average back-calculated damping is lower than the J_t , but higher than the J_s recommended in WEAP for non-cohesive soils. This comparison indicates that the current WEAP recommendations will underpredict the end bearing and overpredict the

shaft resistance in CG-IGMs. Figure 2b shows a non-linear relationship between the back-calculated damping and the combined term of pile penetration length, L (m), and corrected N , $(N_1)_{60}$ (blows/0.3 m) below the pile tip. The nonlinear trend can be best described by the exponential relationship given by Equation (2)

$$\hat{J}_t = \hat{J}_s = 0.07e^{9.3 \frac{L}{(N_1)_{60}}} \tag{2}$$

The predicted \hat{J}_t (s/m) and \hat{J}_s (s/m) from Equation (2) show that the damping factor decreases with increasing $(N_1)_{60}$ of CG-IGMs below the pile tip. Because of limited data points with $8.5 \text{ m} \geq L \leq 14.8 \text{ m}$, $55 \text{ blows}/0.3 \text{ m} \geq (N_1)_{60} \leq 151 \text{ blows}/0.3 \text{ m}$. The pile types used in the development of the prediction equation in Equation (2) include HP 310×79, HP 360×108, and 406-mm open-ended pipe piles (OEP). Future studies are recommended to improve the prediction equation for damping factors by including additional data with longer pile lengths and variable pile types and sizes.

5.4. Subsurface Condition III (Either Soil or Soil-Based IGM as Bearing Layer)

Out of the 34 test piles, 10 fall under subsurface condition III, with the bearing layer identified as either a fine-grained soil-based IGM (FG-IGM), coarse-grained soil-based IGM (CG-IGM), or soil. For the test piles with the FG-IGM or CG-IGM as the bearing layer, this subsurface condition differs from the subsurface conditions I and II due to the presence of both FG-IGM and CG-IGMs along the pile shaft. For piles with soil as the bearing layer, subsurface condition III is identified when FG-IGM, CG-IGM, or both are present as overburden layers. Figure 1 clearly illustrates the identification of subsurface condition III from subsurface conditions I and II. Since damping parameters are found to depend on the subsurface conditions, the application of Equations (1) and (2) is found to be impractical for this condition. The average back-calculated damping factors of 0.33 s/m and 0.59 s/m are recommended for the CG-IGM and FG-IGM layers, respectively, to facilitate the proposed WEAP methods. In addition, the recommended dynamic parameters from the back-calculation study for S-IGMs, along with the default dynamic parameters for soils, are summarized in Table 7 to facilitate the implementation of improved WEAP methods summarized in Table 5.

Table 7. Quake and damping parameters for subsurface conditions I, II, and III.

Subsurface Condition	Geomaterial	Q_s (mm)	Q_t (mm)	J_s (s/m)	J_t (s/m)
I	Soil	2.5	D/120 (very dense/hard soil); D/60 (soft soil)	0.66 (Fine-grained); 0.16 (coarse-grained); 0.33 (silts)	0.5
	FG-IGM		D/120	$\hat{J}_t = \hat{J}_s = 0.05 \frac{S_u \times L}{D_p} - 0.025$	
II	Soil		D/120 (very dense/hard soil); D/60 (soft soil)	0.66 (Fine-grained); 0.16 (coarse-grained); 0.33(silts)	0.5
	CG-IGM		D/120	$\hat{J}_t = \hat{J}_s = 0.07e^{9.3 \frac{L}{(N_1)_{60}}}$	
III	Soil		D/120 (very dense/hard soil); D/60 (soft soil)	0.66 (Fine-grained); 0.16 (coarse-grained); 0.33(silts)	0.5
	CG-IGM				0.59
	FG-IGM	D/120		0.33	

Q_s = Shaft quake; Q_t = Toe quake; J_s = Shaft damping; J_t = Toe damping; D_p = Pile Dimension (mm); D = Pile Diameter (mm); S_u = Undrained shear strength of the bearing layer at the bottom of pile tip (kPa); L = Embedded pile length (m); $(N_1)_{60}$ = Corrected N (b/0.3 m) of the bearing layer at bottom of pile tip; and FG-IGM = Fine grained soil-based IGM; CG-IGM = Coarse-grained soil-based IGM.

6. Determination of Pile Resistances from Bearing Graph Analysis

Bearing graph analyses are conducted to determine the ultimate pile resistances considering all four WEAP methods and three subsurface conditions. The bearing graph analysis procedure for different WEAP methods is illustrated in a flowchart in Figure 3. Each predicted ultimate pile resistance from each WEAP method is compared with the measured pile resistance from CAPWAP at EOD in terms of a resistance bias (λ) where $\lambda > 1$ indicates that WEAP underpredicts the pile resistance and $\lambda < 1$ indicates that WEAP overpredicts the pile resistance. The comparison of the predicted ultimate resistances from each WEAP method and resistances determined from CAPWAP for 34 test piles is shown in Figure 4. Figure 4 shows that WEAP SAD and WEAP UWD, with a mean resistance bias of 1.14, underpredict the pile resistances, on average, by approximately 12%, while the WEAP UWR and WEAP SAR, with a mean bias of 1.02, provide better pile resistance prediction as the mean bias is close to 1. Among the four WEAP methods, WEAP UWR provides better pile resistance prediction as the mean bias is close to unity and the coefficient of variation (COV) of bias is 0.16, the lowest among the four methods.

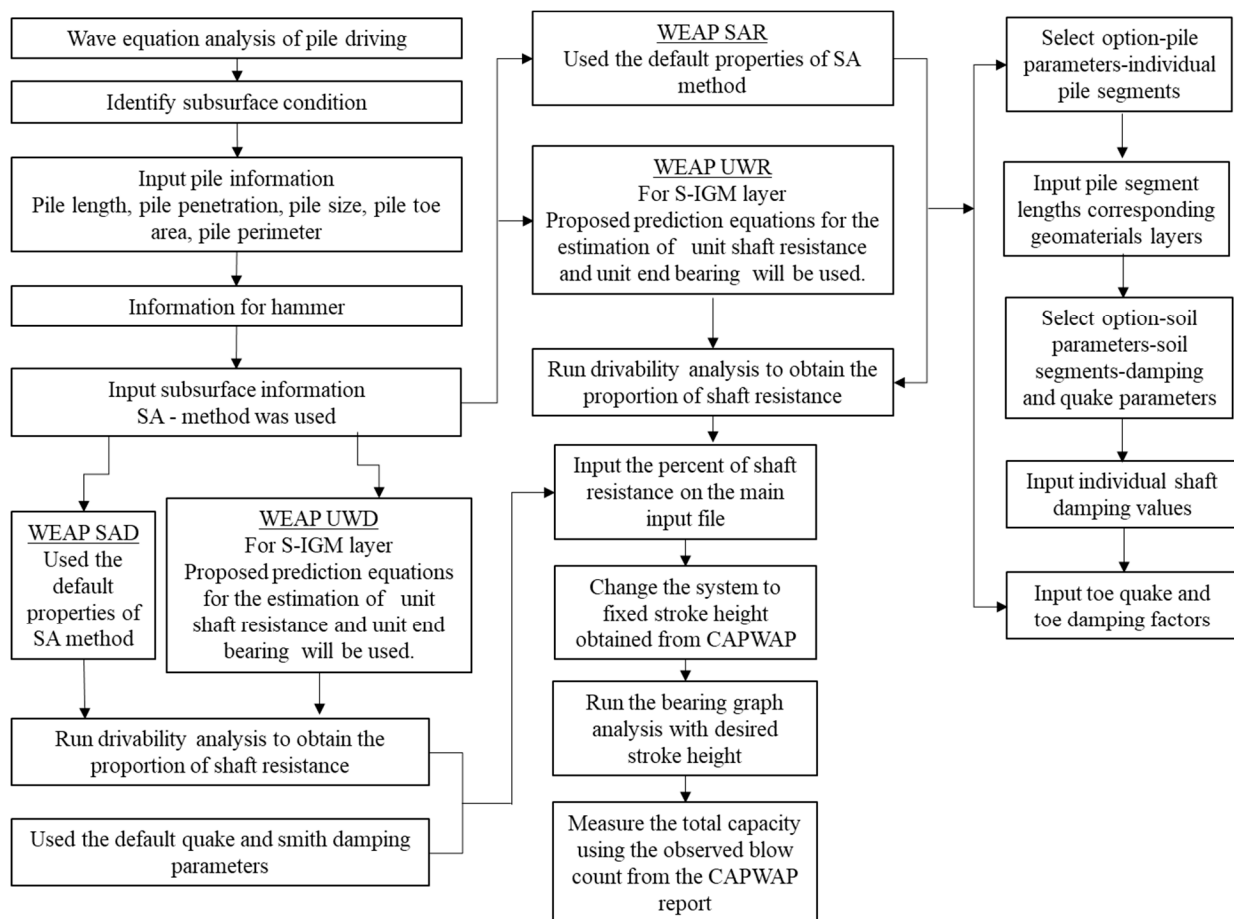


Figure 3. Flowchart comparing the four different WEAP methods.

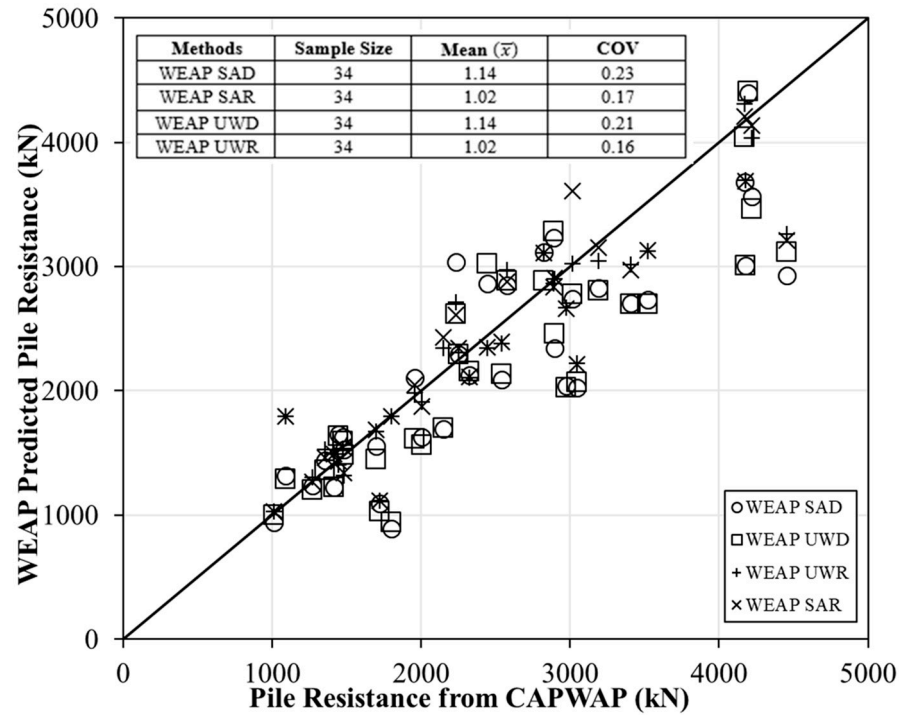


Figure 4. Comparison of measured pile resistances from CAPWAP and predicted pile resistance from WEAP SAD, WEAP UWD, WEAP SAR, and WEAP UWR for the 34-training pile dataset.

7. Validation of Improved WEAP Methods

Twenty-two independent pile data obtained from the pile load test program in Illinois by Long and Anderson [37], as summarized in Table 8, are utilized to validate the improved WEAP methods for predicting pile resistances in subsurface conditions for S-IGMs. Of the 22 test piles, 9 piles are steel H-piles and the remaining 13 test piles are 356-mm diameter close-ended pipe piles. For the bearing IGM layers, 8 test piles are driven in FG-IGM, and 14 test piles are driven in CG-IGM. The classification for CG-IGMs is conducted based on $N \geq 58$ blows/0.3 m, and the classification of FG-IGMs is based on the reported s_u values ≥ 129 kPa following the criteria conducted by Masud et al. [6,22]. Bearing graph analyses are performed using the reported stoke heights and blow counts at the EOD for 22 independent test pile data. The predicted ultimate pile resistances from four different WEAP methods are compared with those from CAPWAP in Figure 5. The mean and COV of resistance biases for the four WEAP methods are included in Figure 5 for comparative study. The highest COV of 0.25 is obtained from the WEAP SAD and WEAP UWD methods. Having the mean resistance bias of 1.04, the pile resistances are underpredicted by the WEAP SAD and WEAP UWD, on average, by only approximately 4%. However, the WEAP UWR and WEAP SAR improve the pile resistance predictions by reducing the underprediction of pile resistances by around 5% (from 1.04 to 0.99) and the COV by 20% (from 0.25 to 0.20).

Considering the different environmental conditions outside the study’s geographical scope, WEAP UWR is the best method of four for pile resistance prediction with a mean bias closer to 1 and the lowest COV of 0.20.

This WEAP UWR method incorporates the newly proposed damping parameters and static analysis methods and provides more consistent resistance estimation compared to other methods (Figure 5). The same observations of the mean close to unity and lower COV are obtained for WEAP UWR methods based on 34 training test pile data (Figure 4).

Table 8. Summary of independent test pile data and relevant End of Driving (EOD) information for validation.

Site	Location	Pile Type	L (m)	Bearing Geo-Material	EOD Information			
					S (m)	B	R _m	Hammer
Jules	SW wing, Pile 1	HP 310×79	7.8	FG-IGM	2.5	48	589.6	Delmag D 8-32
I-78 Over S.	HP	HP 360×132	19.5	CG-IGM	1.8	30	1337.7	Delmag D 36-32
	Pile 3	CEP 356 mm	8.5	CG-IGM	1.9	42	843.7	Delmag D 25-32
Greenville	Pile 12	CEP 356 mm	6.7	CG-IGM	2.2	17	845.9	Delmag D 36-32
	Pile 13	CEP 356 mm	15.2	FG-IGM	2.2	33	1438.7	Delmag D 25-32
Mahomet	North Abt.	HP 360×108	20.7	CG-IGM	2.1	126	2553.9	Delmag D 30-32
	South Abt.	HP 360×108	12.6	CG-IGM	2.2	42	1276.3	Pileco D 19-42
	Pier 2	HP 360×108	15.2	CG-IGM	2.5	81	2833.3	Delmag D 30-32
Godfrey	West Abt.	CEP 356 mm	12.5	FG-IGM	2.6	52	1012.4	Delmag D 12-32
Bloomington	K-pile	HP 310×93	30.8	CG-IGM	2.4	115	1367.9	APE D 19-42
Panther creek	South Abt.	HP 250×85	12.0	CG-IGM	2.7	144	1599.8	ICE 42-S
	East Abt.	CEP 356 mm	17.7	CG-IGM	2.1	37	763.6	MKT DE 42
	Pier	CEP 356 mm	16.0	CG-IGM	2.5	49	1416.9	MKT DE 42
Oquawka	West Abt.	CEP 356 mm	20.1	FG-IGM	2.3	22	645.3	MKT DE 42
	North Abt.	CEP 356 mm	16.6	FG-IGM	2.7	40	1367.9	Delmag D 19-42
	Pier 1	CEP 356 mm	21.0	FG-IGM	2.9	34	833.0	Delmag D 19-42
Stronghurst	Pier 2	CEP 356 mm	17.2	CG-IGM	2.7	38	1288.7	Delmag D 19-42
	Pier 1	HP 310×93	11.9	FG-IGM	2.4	120	1651.8	Delmag D 19-32
Jacksonville	Pier 2	HP 310×93	19.0	FG-IGM	2.1	200	1376.8	Delmag D 19-32
	North Abt.	CEP 356 mm	11.9	CG-IGM	2.2	90	1596.7	Delmag D 19-32
RCS Godfrey	North pier	CEP 356 mm	9.0	CG-IGM	1.8	72	977.7	Delmag D 19-32
	South pier	CEP 356 mm	5.9	CG-IGM	2.1	81	1579.8	Delmag D 19-32

L = Penetration length; Abt. = Abutment; S = Stroke height; B = Blow count (blows/ft); EOD = End of Driving; R_m = CAPWAP measured pile capacity at EOD; CEP = Close ended pipe pile; SW = South-west; S. = Sangamon.

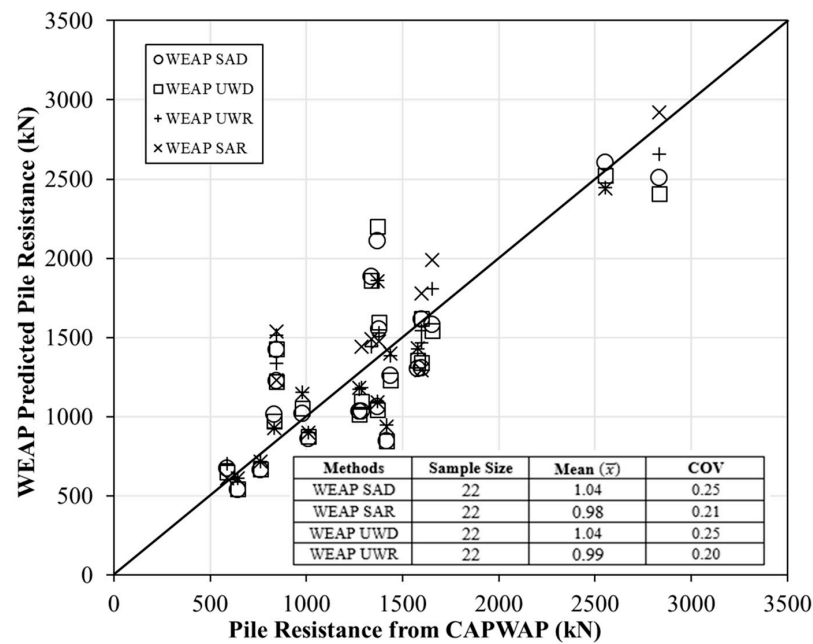


Figure 5. Comparison of measured pile resistances from CAPWAP and predicted pile resistances from WEAP SAD, WEAP UWD, WEAP SAR, and WEAP UWR for the 22 independent pile data.

8. LRFD Resistance Factors

The resistance factors (ϕ) for WEAP, as recommended by the AASHTO [38], are developed initially for piles driven in soils. To ascertain the reliability of WEAP on pile resistance predictions, LRFD resistance factors are calibrated to reflect the uncertainty associated with the resistance prediction of driven piles in S-IGMs. Improved pile design reliability is obtained by limiting the database to a particular geologic region and corresponding construction practices [38]. LRFD resistance factor values are calibrated using FOSM, FORM, and MCS.

The efficiency of the different WEAP methods is assessed using efficiency factors ($\frac{\phi}{\bar{x}}$), which are established at reliability indexes (β_T) of 2.33 and 3.0 for a redundant pile group and a non-redundant pile group, respectively [39]. The calibration of resistance factors using FOSM, FORM, and MCS required the mean, standard deviation, and COV of resistance biases. The details of the calibration procedures are discussed in the literature [39,40].

The ϕ values are calibrated using the 34 training test piles and 22 independent test piles used in the validation. The Shapiro–Wilk (SW) [41] test and Anderson–Darling (AD) [42] test are performed to assess whether the resistance biases meet the assumptions of Normality or Log-Normality. A significance level of p value = 0.05 is used for these normality tests. The results of the normality tests are summarized in Table 9. For the WEAP SAD and WEAP UWD, no violation of the Normal and Log-Normal distribution assumptions is detected because the P -values are greater than 0.05. However, for WEAP UWR and WEAP SAR, both the Normal and the Log-Normal distribution assumptions are rejected by SW and AD tests as their P -values are less than 0.05. Test piles are identified as outliers if the difference between λ and exceeds twice the standard deviation. These outliers are then excluded to improve the quality of the calibrated ϕ [39]. The normality test results after removing the outliers (Table 9) showed that both the Normal and Log-Normal distribution assumptions were not violated. Thus, the Log-Normal distribution is selected in the LRFD resistance factor calibration based on the higher Log-likelihood value.

Table 9. Results from the Shapiro–Wilk and Anderson–Darling tests.

Method	Sample Size	Mean (\bar{x})	COV	Normal		Log-Normal		Log-Likelihood	
				SW	AD	SW	AD	Normal	Log-Normal
				p -Value					
WEAP SAD	56	1.10	0.24	0.08	0.22	0.90	0.62	−4.99	−2.86
WEAP UWD	56	1.11	0.23	0.10	0.13	0.46	0.24	−2.21	−1.05
WEAP UWR	56	1.02	0.18	0.007	0.003	0.001	0.000	NA	NA
WEAP SAR	56	1.01	0.19	0.005	0.03	0.03	0.02	NA	NA
WEAP SAD *	54	1.08	0.21	0.76	0.70	0.32	0.33	3.28	4.23
WEAP UWD *	54	1.08	0.21	0.08	0.25	0.19	0.11	2.58	2.90
WEAP UWR *	50	1.02	0.12	0.08	0.13	0.26	0.15	33.49	34.04
WEAP SAR *	51	1.00	0.14	0.23	0.28	0.65	0.52	29.07	29.80

n = Sample size; (\bar{x}) = Mean resistance bias; COV = Coefficient of Variation; SW = Shapiro Wilk’s test; AD = Anderson Darling test; p = p -value of normality test; NA = Not applicable; * = No outliers.

Table 10 summarizes the resistance and efficiency factors for the four WEAP methods. The ϕ values of WEAP SAD and WEAP UWD vary from 0.70 to 0.82, while higher ϕ values ranging from 0.72 to 0.94 are calibrated for WEAP UWR and WEAP SAR at $\beta_T = 2.33$. Compared with $\phi = 0.50$ recommended in the AASHTO [38] for soils, the calibrated ϕ values using FOSM at $\beta_T = 2.33$ for piles in S-IGMs are 40%, 40%, 44%, and 50% higher for WEAP SAD, WEAP UWD, WEAP SAR, and WEAP UWR, respectively. The obtained resistance factors are also higher than the $\phi = 0.40$ recommended by Paikowsky et al. [40]. These higher calibrated ϕ values are attributed to mean bias closer to one and lower COV

values. In this study, φ values based on FORM and MCS, on average, are 17%, 17%, 22%, and 24% higher than that from FOSM for WEAP SAD, WEAP UWD, WEAP SAR, and WEAP UWR, respectively, for $\beta_T = 2.33$. Among all the different methods, WEAP UWR has the highest resistance and efficiency factors. The values of φ for the WEAP UWR are, on average, 12% higher than those for the default WEAP SAD methods for $\beta_T = 2.33$. In addition, the efficiency factor of the WEAP UWR, on average, is approximately 20% higher than the WEAP SAD for $\beta_T = 2.33$. Compared with the default WEAP SAD, the selected proposed WEAP UWR method, on average, reduces the underprediction of pile resistances by 6% and improves the reliability with a 43% reduction in the coefficient of variation (COV) for $\beta_T = 2.33$.

Table 10. Calibrated resistance factors for WEAP analysis on driven piles in soil-based IGMs.

Method	FOSM				FORM				MCS			
	$\beta_T = 2.33$		$\beta_T = 3.00$		$\beta_T = 2.33$		$\beta_T = 3.00$		$\beta_T = 2.33$		$\beta_T = 3.00$	
	φ	$\frac{\varphi}{(\bar{x})}$										
WEAP SAD	0.70	0.64	0.57	0.52	0.82	0.75	0.70	0.64	0.82	0.75	0.69	0.63
WEAP UWD	0.70	0.64	0.57	0.52	0.82	0.75	0.70	0.64	0.82	0.75	0.69	0.63
WEAP UWR *	0.75	0.74	0.64	0.63	0.94	0.92	0.84	0.82	0.93	0.91	0.83	0.81
WEAP SAR	0.72	0.72	0.61	0.61	0.88	0.88	0.79	0.79	0.88	0.88	0.77	0.77

FOSM = Factor of Safety Method; FORM = First Order Reliability Method; MCS = Monte Carlo Simulation; β_T = Reliability index; φ = Resistance factor; $\frac{\varphi}{(\bar{x})}$ = Efficiency factor; * = Selected proposed method.

9. Economic Impact Assessment

In this section, an economic impact study is conducted between default WEAP SAD and WEAP UWR methods. The WEAP UWR is chosen for this economic impact study because it exhibits the mean value closest to unity and lowest COV values based on the bearing graph analysis and the highest LRFD resistance factors. This economic study is limited to determining the discrepancies in the number of test piles observed during the construction of individual projects. However, other factors such as life cycle cost analysis, risk assessment, and corrosion assessment of steel piles can be considered in future studies. Figure 6 shows the flowchart explaining the economic impact assessment in the following steps:

Step 1. The factored load per pile (γQ) is multiplied by the number of piles per pier or abutment to determine the overall load demand at each pier or abutment site.

Step 2. Using the suggested resistance factor of 0.65 from AASHTO [38], the total factored resistance per pile from CAPWAP (φR_C) is determined.

Step 3. Determine factored pile resistance (φR_D) for the default WEAP SAD using $\varphi = 0.5$ [38]. The WEAP SAD resistances are obtained from the bearing graph based on the stoke height and blow count at the EOD condition.

Step 4. Determine the factored pile resistances (φR_P) for the WEAP UWR method using $\varphi = 0.75$ based on FOSM at $\beta_T = 2.33$.

Step 5. The number of piles to satisfy the LRFD strength limit state ($\gamma Q \leq \varphi R$) is determined by dividing the total load demand from Step 1 by the φR_C from Step 2, φR_D from Step 3, or φR_P from Step 4.

Step 6. Compute the differences in pile numbers between the WEAP and CAPWAP, showing whether pile resistance is overestimated or underestimated.

Step 7. Convert the differences in pile numbers into equivalent steel weight per unit load for comparison, considering the type of pile and its penetration length.

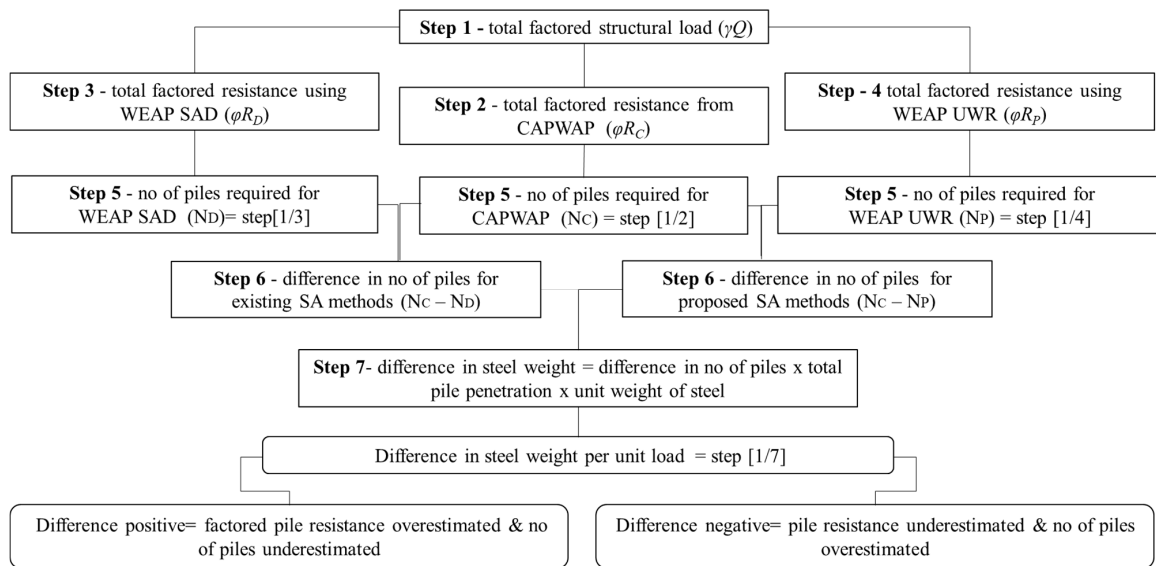


Figure 6. A flow chart showing the methodology for economic impact assessment.

Following these steps, the economic impact assessment is conducted only for the first 32 test piles shown in Table 5 because pile numbers 33 and 34 do not have the reported load demand. The validation dataset for the piles driven in S-IGMs is not used as the structural load demand is not reported. Figure 7 shows the difference in steel weight for 32 test piles for both the WEAP SAD and WEAP UWR methods. The average differences in steel weight per unit load for the WEAP SAD and WEAP UWR are -0.54 kg/kN and 0.06 kg/kN, respectively. If the WEAP SAD method had been used as the construction control method instead of CAPWAP, it would have highly underestimated pile resistance and resulted in overestimating the number of piles.

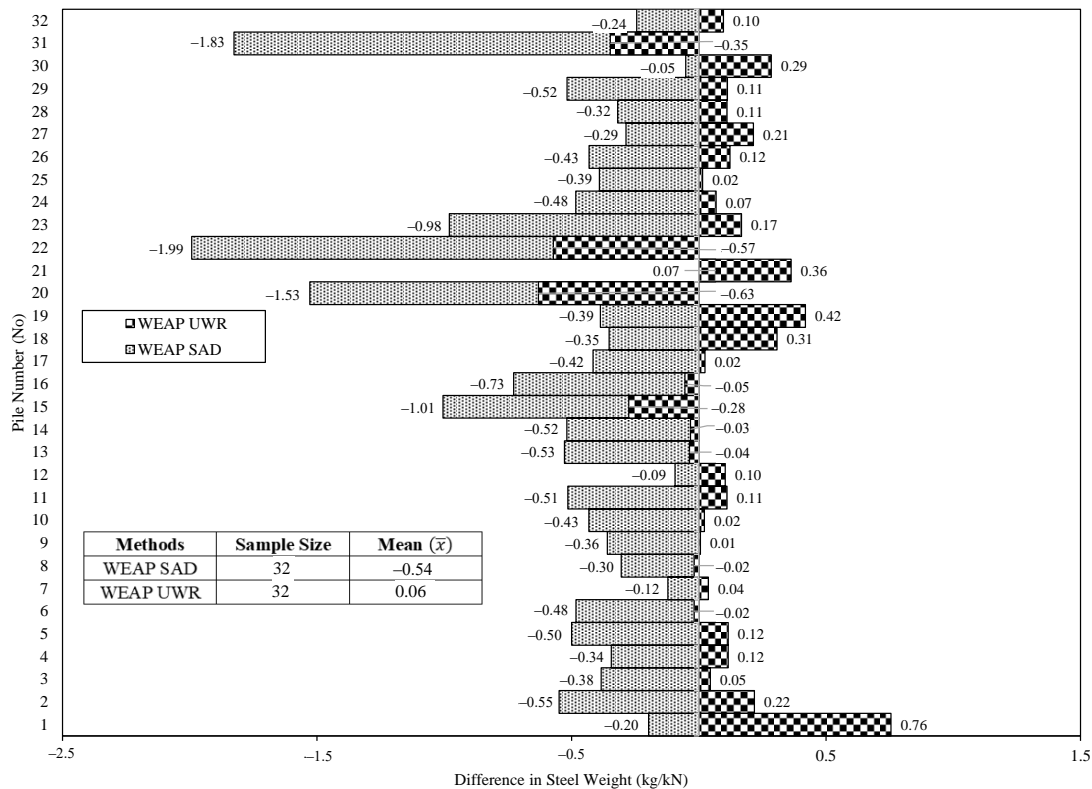


Figure 7. Plot of the differences in steel weight based on the WEAP SAD and WEAP UWR methods.

This overestimation of the number of piles could create cost overrun during the construction phase due to excess steel piles used. Alternatively, if the WEAP UWR is used, there is a slight overestimation of the pile resistance, leading to a slight underestimation of several WEAP SAD methods; the WEAP UWR method seems to be more efficient as the average difference in steel weight per unit load is closer to zero.

10. Summary and Conclusions

Thirty-four test piles driven into S-IGMs from four states are used in this study to develop a new procedure for WEAP analysis to improve the prediction of pile resistances in S-IGMs. The back-calculation of the dynamic parameters for the S-IGMs is performed by matching the predicted ultimate pile resistance from WEAP with the resistance determined from CAPWAP at the EOD. This study focuses on improved WEAP analysis for steel piles driven into soil-based IGMs only. However, the same methodologies can be adopted for other pile materials and types to develop new damping parameters and WEAP methods. The economic impact assessment conducted in this study is limited to performance analysis in terms of the number of differences in steel weight. However, different pile types, maintenance, and long-term performance can be considered in future studies. Subsurface variability and uncertainty are also important factors that are not considered in this study but are suggested for future studies. The study yields the following conclusions:

- Quake values of 2.5 mm and $D/120$ for Q_s and Q_t , respectively, are adequate for the S-IGMs. Smith damping factors are found to depend on the pile driving and subsurface conditions. Single values of Smith damping factors are inadequate for different pile and driving conditions. Hence, new Smith damping factors are proposed for three different subsurface conditions.
- Using 34 training pile test data and 22 independent test pile data, it is found that WEAP UWR is the most efficient as it provides a mean resistance bias of 1.02 closer to 1 and the lowest COV of 0.18.
- A ϕ value of 0.75 for WEAP UWR calibrated based on FOSM at $\beta_T = 2.33$ for piles driven into S-IGMs is higher than the value of ϕ of 0.5 recommended in AASHTO [38] for piles in soils. Compared with the default WEAP SAD, the selected proposed WEAP UWR method, on average, reduces the underprediction of pile resistances by 6% and improves the reliability with a 43% reduction in the coefficient of variation (COV) for $\beta_T = 2.33$.
- The economic impact assessment reveals that the average differences in steel weight per unit load for the WEAP SAD and WEAP UWR are -0.54 kg/kN and 0.06 kg/kN, respectively. Compared with the WEAP SAD method, the WEAP UWR method seems to be more efficient as the average difference in steel weight per unit load is closer to zero, which will reduce construction challenges.

Author Contributions: The authors confirm contributions to the paper as follows: study conception and design: H.K.K., K.N. and N.B.M.; data collection: N.B.M. and H.K.K.; analysis and interpretation of results: H.K.K., K.N. and N.B.M.; draft manuscript preparation: N.B.M., H.K.K., K.N. and S.S.W. All authors have read and agreed to the published version of the manuscript.

Funding: The research was supported by Wyoming Department of Transportation as the lead agency under the Grant RS05219.

Data Availability Statement: All data and materials are available on request from the corresponding author. The data are not publicly available due to ongoing researches using a part of the data.

Acknowledgments: The authors express their sincere gratitude to research supports from the Wyoming Department of Transportation, the Colorado Department of Transportation, the Iowa Department of Transportation, the Kansas Department of Transportation, the North Dakota Department of Transportation, the Idaho Transportation Department, and the Montana Department of Transportation.

Conflicts of Interest: The State of Wyoming, WYDOT, and University of Wyoming reserve a royalty-free, nonexclusive, unlimited, and irrevocable license to reproduce, published, or otherwise use, and to authorize others to use the copyright in any work that is generated from the research project entitled Wyoming, Comprehensive Field Load Test and Geotechnical Investigation Program for Development of LRFD Recommendations of Driven Piles on Intermediate Geomaterials, TPF 5-391.

References

1. Santi, P.M.; Doyle, B.C. The Locations and Engineering Characteristics of Weak Rock in the US. In *Characterization of Weak and Weathered Rock Masses*; Santi, P.M., Shakoor, A., Eds.; Association of Engineering Geologists Special Publication 9; Association of Engineering Geologists: Denver, CO, USA, 1997; pp. 1–22.
2. Clarke, B.G.; Smith, A. Self-boring Pressuremeter Tests in Weak Rocks. In *Construction and Building Materials*; Elsevier: Amsterdam, The Netherlands, 1992; Volume 6, pp. 91–96.
3. Marinou, P.G. Hard Soils-Soft Rocks: Geological Features with Special Emphasis to Soft Rocks. In *Geotechnical Engineering of Hard Soils-Soft Rocks*; A.A. Balkema: Brookfield, The Netherlands, 1997; pp. 1807–1818.
4. De Freitas, H. Introduction to Session 1.2: Weak Arenaceous Rock. In Proceedings of the 26th Annual Conference of the Engineering Group Geological Society, Leeds, UK, 9–13 September 1993; pp. 115–123.
5. Martin, D.; Stacey, P. *Guidelines for Open Pit Slope Design in Weak Rocks*; CSIRO Publishing: Clayton, Australia, 2018.
6. Mokwa, R.L.; Brooks, H. *Axial Capacity of Piles Supported on Intermediate Geomaterials*; Final Report No. FHWA/MT-08-008/8117-32; Western Transportation Institute, Montana State University: Bozeman, MT, USA, 2008.
7. Masud, N.B.; Ng, K.W.; Wulff, S.S.; Johnson, T. Driven Piles in Fine Grained Soil-based Intermediate GeoMaterials. *J. Bridge Eng.* **2022**, *27*, 04022037-1-13. [[CrossRef](#)]
8. Masud, N.B.; Ng, K.W.; Wulff, S.S. New Static Analysis Methods for the Prediction of Driven Pile Resistance in Siltstone. In Proceedings of the Geo-Congress 2022, Geotechnical Special Publication No. 332, ASCE, Charlotte, NC, USA, 20–23 March 2022; pp. 93–103.
9. Masud, N.B.; Ng, K.W.; Kalauni, H.K.; Wulff, S.S. Reliability-based design improvement and prediction of steel driven pile resistances in rock-based intermediate geomaterials. *Acta Geotech.* **2023**, *19*, 1083–1105. [[CrossRef](#)]
10. Islam, M.S.; Ng, K.W.; Wulff, S.S. Improved wave equation analysis of steel H-piles in shales considering LRFD and Economic Impact Studies. *J. Bridge Eng.* **2022**, *27*, 04022039-1-13. [[CrossRef](#)]
11. Islam, M.S. Pile Behaviors in Shales through Full-Scale Static Load Testing, Dynamic Testing, and Finite Element Analysis. Master's Thesis, Department of Civil and Architectural Engineering, University of Wyoming, Laramie, WY, USA, 2021.
12. Long, H.J. *Static Pile Load Tests on Driven Piles in Intermediate Geomaterials*; Project No. 0092-12-08; Wisconsin Highway Research Program: Madison, WI, USA, 2016.
13. Masud, N.B.; Ng, K.W.; Oluwatuyi, O.E.; Islam, M.S.; Kalauni, H.K.; Wulff, S.S. Evaluation of Static Load Test Systems for Driven Piles in Intermediate GeoMaterials. *Transp. Res. Rec.* **2023**, *2677*, 741–756. [[CrossRef](#)]
14. Doherty, P.; Igoe, D. A driveability study of precast concrete piles in dense sand. *DFI J.-J. Deep Found. Inst.* **2013**, *7*, 3–16. [[CrossRef](#)]
15. Rausche, F.; Nagy, M.; Webster, S.; Liang, L. CAPWAP and refined wave equation analyses for driveability predictions and capacity assessment of offshore pile installations. In Proceedings of the International Conference on Offshore Mechanics and Arctic Engineering, Honolulu, HI, USA, 31 May–5 June 2009; Volume 43475, pp. 375–383.
16. Schneider, J.A.; Ivy, A.H. Analyzing drivability of open ended piles in very dense sands. *DFI J.-J. Deep Found. Inst.* **2010**, *4*, 32–44. [[CrossRef](#)]
17. Ramey, G.E.; Hudgins, A.P. Sensitivity and Accuracy of the Pile Wave Equation. *Ground Eng.* **1977**, *10*, 45–47.
18. Coyle, H.M.; Bartoskewitz, R.E.; Berger, W.J. *Bearing Capacity by Wave Equation Analysis—State of Art*; Texas Transportation Institute, Texas A&M University: College Station, TX, USA, 1973.
19. Raines, R.D.; Ugaz, O.G.; O'Neill, M.W. Driving characteristics of open-toe piles in dense sand. *J. Geotech. Eng.* **1992**, *118*, 72–88. [[CrossRef](#)]
20. Bartoskewitz, R.E.; Coyle, H.M. *Wave Equation Prediction of Pile Bearing Capacity Compared with Field Test Results*; Research Report 125-5; Texas Transportation Institute, Texas A&M University: College Station, TX, USA, 1970.
21. Rausche, F.; Thendean, G.; Abou-Matar, H.; Likins, G.E.; Goble, G.G. *Determination of Pile Driveability and Capacity from Penetration Tests, Volume I (No. FHWA-RD-96-179)*; Department of Transportation, Federal Highway Administration: Washington, DC, USA, 1997.
22. Iskander, M.G.; Stachula, A. Wave equation analyses of fiber-reinforced polymer composite piling. *J. Compos. Constr.* **2002**, *6*, 88–96. [[CrossRef](#)]
23. Ta, A.N.; Hammann, M. Application of adjusted wave equation analysis for optimized pile acceptance criteria. In Proceedings of the 5th International Young Geotechnical Engineers' Conference, Paris, France, 31 August–1 September 2013; pp. 230–233.
24. Masud, N.B.; Ng, K.W.; Wulff, S.S. Resistance responses and design recommendations for driven piles in coarse-grained soil-based intermediate geomaterials. *Soils Found.* **2023**, *63*, 101381. [[CrossRef](#)]
25. Pile Dynamics, Inc. *GRLWEAP Manual for Windows*; Pile Dynamics, Inc.: Cleveland, OH, USA, 2010.
26. Smith, T.; Banas, A.; Gummer, M.; Jin, J. *Recalibration of the GRLWEAP LRFD Resistance Factor for Oregon DOT*; No. FHWA-OR-RD-11-08; Research Unit, Oregon Department of Transportation: Salem, OR, USA, 2011.

27. Smith, E.A.L. Pile-Driving Analysis by the Wave Equation. *Trans. Am. Soc. Civ. Eng.* **1962**, *127*, 1145–1171. [[CrossRef](#)]
28. Goble, G.G.; Rausche, F. *Wave Equation Analysis of Pile Driving—WEAP Program Manual*; Report No. FHWA IP-76-14.1 through IP-76-14.4; U.S. Department of Transportation: Washington, DC, USA, 1976; Volume 1–4.
29. Lawton, E.C.; Fragaszy, R.J.; Higgins, J.D.; Kilian, A.P.; Peters, A.J. *Review of Methods for Estimating Pile Capacity*; No. 1105: Structure Foundations; Transportation Research Board: Washington, DC, USA, 1986; pp. 32–40.
30. Forehand, P.W.; Reese, J.L. Prediction of capacity by the wave equation. *J. Soil Mech. Found. Div. ASCE* **1964**, *90*, 1–26. [[CrossRef](#)]
31. Liang, R.Y.; Sheng, Y. Wave Equation Parameters from Driven-Rod Test. *J. Geotech. Eng.* **1993**, *119*, 1037–1057. [[CrossRef](#)]
32. McVay, M.C.; Kuo, C.L. *Estimate Damping and Quake by Using Traditional Soil Testing*; Department of Civil Engineering, University of Florida: Gainesville, FL, USA, 1999.
33. Coyle, H.M.; Gibson, G.C. Closure to Empirical Damping Constants for Sands and Clays. *J. Soil Mech. Found. Div.* **1970**, *97*, 1487–1488. [[CrossRef](#)]
34. Hannigan, P.J.; Goble, G.G.; Thendean, G.; Likins, G.E.; Rausche, F. *Design and Construction of Driven Pile Foundations—Volume II*; FHWA-HI-97-013; National Highway Institute, Federal Highway Administration, U.S. Department of Transportation: Washington, DC, USA, 1998.
35. Adhikari, P. Load and Resistance Factor Design and Construction Control of Driven Piles in Intermediate Geomaterials. Ph.D. Dissertation, Department of Civil and Architectural Engineering, University of Wyoming, Laramie, WY, USA, 2019.
36. Smith, E.A.L. Pile driving analysis by the wave equation. American Society of Civil Engineers. *ASCE J. Soil Mech. Found. Eng.* **1960**, *86*, 35–61. [[CrossRef](#)]
37. Long, J.; Anderson, A. *Improved Design for Driven Piles on a Pile Load Test Program in Illinois*; Research Report FHWA-ICT-12-011; Center for Transportation: Urbana, IL, USA, 2012.
38. AASHTO. *AASHTO LRFD Bridge Design Specifications*, 9th ed.; U.S. Customary Units. American Association of State Highway and Transportation Officials (AASHTO): Washington, DC, USA, 2020.
39. Bougataya, Y.; Stuedlein, A.W. Region-specific calibration of resistance factors for use with static and wave equation analyses of driven piles. *DFI J.-J. Deep Found. Inst.* **2016**, *10*, 143–152. [[CrossRef](#)]
40. Paikowsky, S.G.; Birgisson, B.; McVay, M.; Nguyen, T.; Kuo, C.; Baecher, G.; Ayyab, B.; Stenersen, K.; O'Malley, K.; Chernauskas, L.; et al. *Load and Resistance Factor Design (LRFD) for Deep Foundations*; NCHRP Report No. 507; Transportation Research Board of the National Academics: Washington, DC, USA, 2004.
41. Schwarz, G. Estimating the dimension of a model. *Ann. Stat.* **1978**, *6*, 461–464. [[CrossRef](#)]
42. Anderson, T.W.; Darling, D.A. Asymptotic Theory of Certain Goodness-of-fit Criteria based on Stochastic Processes. *Ann. Math. Stat.* **1952**, *23*, 193–212. [[CrossRef](#)]

Disclaimer/Publisher's Note: The statements, opinions and data contained in all publications are solely those of the individual author(s) and contributor(s) and not of MDPI and/or the editor(s). MDPI and/or the editor(s) disclaim responsibility for any injury to people or property resulting from any ideas, methods, instructions or products referred to in the content.